Accepted Manuscript

Tribological and mechanical properties of graphene nanoplatelet/PEEK composites

J.A. Puértolas, M. Castro, J.A. Morris, R. Ríos, A. Ansón-Casaos

PII: S0008-6223(18)30850-9

DOI: 10.1016/j.carbon.2018.09.036

Reference: CARBON 13464

To appear in: *Carbon*

Received Date: 12 April 2018

Revised Date: 18 July 2018

Accepted Date: 9 September 2018

Please cite this article as: J.A. Puértolas, M. Castro, J.A. Morris, R. Ríos, A. Ansón-Casaos, Tribological and mechanical properties of graphene nanoplatelet/PEEK composites, *Carbon* (2018), doi: 10.1016/j.carbon.2018.09.036.

Tribological and Mechanical Properties of Graphene Nanoplatelet/PEEK Composites

J.A. Puértolas[1]*, M. Castro[2], J.A. Morris[1], R. Ríos[1], A. Ansón-Casaos[3]

[1]Instituto de Investigación en Ingeniería de Aragón, I3A, Universidad de Zaragoza, 50018 Zaragoza, Spain
[2]Instituto de Ciencia de Materiales de Aragón, ICMA, CSIC-Universidad de Zaragoza, 50009 Zaragoza, Spain
[3]Instituto de Carboquímica, ICB-CSIC, Miguel Luesma Castán 4, 50018 Zaragoza, Spain

*Corresponding author. E-mail: japr@unizar.es (José Antonio Puértolas)
Tel. : +34 976 762521
Fax. : +34 976 761957

Graphene/PEEK composite

Wear reduction

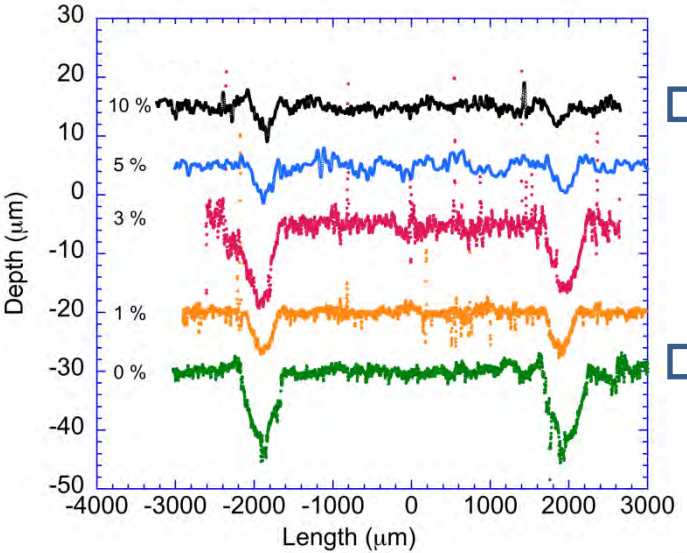

Wear mechanism

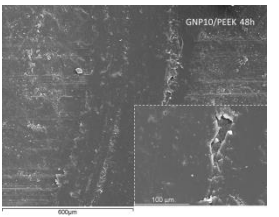

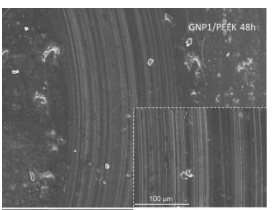

ABSTRACT

Poly(ether ether ketone) (PEEK) is a relevant thermoplastic in industry and in the biomedical sector. In this work, the lubricant capability of graphene nanoplatelets (GNPs) is used for improving the PEEK wear properties. Nanocomposites were prepared by solvent-free melt-blending and injection molding at various compositions between 1 and 10 wt. % of GNPs. The Raman G band shows a progressive increment proportional to the bulk GNP percentage. From calorimetric data, the polymer matrix structure is interpreted in terms of a 3-phase model, in which the crystalline phase fluctuates from 39 to 34% upon GNP addition. Thermal conductivity varies in accordance with the polymer crystallinity. Tensile and flexural tests show a progressive increase in the modulus, as well as a decrease in the fracture strength and the work of fracture. Most important, the composite surface undergoes a substantial improvement in hardness (60%), together with a decrease in the coefficient of friction (-38%) and a great reduction in the wear factor (-83%). Abrasion and fatigue wear mechanisms are predominant at the lowest and highest GNP concentrations respectively. In conclusion, GNPs are used without any chemical functionalization as the filler in PEEK-based materials, improving the surface hardness and the tribological properties.

KEYWORDS: Poly(ether ether ketone); graphene; friction; wear; hardness.

1. Introduction

Poly(ether ether ketone) (PEEK) is a polymer with high thermal and chemical stability, good mechanical performance and suitable tribological characteristics. The PEEK properties originate from the aromatic structure of the polymer chain and its semi-crystalline character, which depends on the thermomechanical processing history. These properties, combined with an easy manufacture, allow the PEEK utilization in different mechanical elements such as piston parts, pumps, bearing mechanisms, and so on. Besides, its biocompatibility and transparency to radiation have allowed the implementation as a biomaterial for trauma, spine, and orthopedic applications [1].

In order to further improve the PEEK properties, in particular wear resistance, frictional losses, mechanical properties and osteointegration, different strategies have been followed [2, 3]. The most common method is based on reinforcing the polymer with different fillers, whose composition, size, concentration, orientation and shape are specific for the required property. Some of the tested fillers have been glass-fibers [4], hydroxyapatite [5], carbon-fibers [6] or carbon nanotubes [7-9].

The use of graphene as a filler in polymers is justified by its high intrinsic performance in terms of stiffness and mechanical resistance, given by its high elastic modulus of 1 TPa and tensile strength of 130 GPa [10, 11]. In addition, graphene offers a large surface area that should provide wide interfaces with the matrix, increasing the load transfer capability and thus the composite strength. Concerning chemical stability, the presence of a network of conjugated double bonds provides a large electron donor–acceptor capacity with the ability to easily react with free radicals [12]. Finally, the two-dimensional structure of graphene points to its potential use as a high-performance solid lubricant, an additive in liquid lubricants [13] and a sliding coating layer [14].

Several works in the literature have assessed the influence of graphene fillers on the tribological and mechanical properties of different polymers, such as polyacrylonitrile [15], poly(vinyl chloride) [16], polyimide [17], polytetrafluorethylene (PTFE) [18] and ultrahigh molecular weight polyethylene [19]. However, only a few works have appeared about graphene/PEEK composites [20-23]. Some of them incorporate graphene oxide (GO) [21], instead of the graphene nanoplatelets (GNPs) used in this work. Others are based on industrially unusual manufacturing processes, such as low-temperature sintering methods [20], or prepare complex hybrid composites with PEEK, short carbon fibers (SCFs) and PTFE [22].

The aim of this work is to get GNP/PEEK composites with high stiffness and strength, together with low coefficients of friction and wear factors. The new materials are considered in order to improve the mechanical and tribological performance of PEEK in its current industrial applications. They could also open new biomedical applications towards the substitution of metallic components in total joint replacements, temporomandibular joints, removable partial dentures, cervical cages, bone plate structures and screws, and total facet arthroplasties [24]. Moreover, we restrict the composite consolidation to industrial processes, with no use of solvents in the different fabrication steps and without functionalization of the filler, allowing potential uses in the strictest sectors such as the biomedical one, and significantly reducing the economic cost of the composite. In this work, we assess the optimal filler concentration to obtain the best wear resistance, maintaining a suitable mechanical performance. Furthermore, the influence of bare GNP fillers on PEEK composites is comprehensively studied concerning the microstructural, thermal, mechanical and tribological properties.

2. Materials and Methods

2.1. Materials

PEEK was provided in a pellet form by Victrex plc, UK (150P grade, M_w = 40000 g/mol, half-step glass transition temperature T_g = 147°C, melting temperature T_m = 345°C, density ρ = 1.30 g/cm^3 at 25 °C). Pellets were dried at 150°C prior to their use. The GNPs were supplied by Avanzare, Spain (avanPLAT-40® grade). This GNP powder material is produced by mechanical exfoliation of graphite, resulting in an average lateral size of 40 μm, thickness around 10 nm, and a number of stacked layers ≤ 30. Composites with different nanofiller concentrations were prepared and denoted as GNPx/PEEK, where x is the filler weight percentage.

2.2. Composite preparation

Melt blending of the PEEK nanocomposites was performed in an industrial extrusion-compounding machine (Coperion ZSK 26 by Coperion GmbH, Germany) equipped with a 26 mm diameter co-rotating twin-screw and two Brabender gravimetric feeders. The temperature of the extruder was set at 330ºC at the feeder, increasing up to 360ºC at the nozzle. A screw profile of high shear rate was used in order to ensure a proper dispersion, with a rotor speed of 250 rpm. The PEEK dosage was set at 10 kg/h, and different quantities of GNPs were dosed through a lateral feeder in order to achieve final concentrations of 1, 3, 5 and 10 wt.% in the nanocomposites. The molten material was extruded through a 2 mm diameter die at a constant output rate. The extrudate strand was quenched immediately in a water bath at room temperature, dried and cut into small pellets. Pure PEEK material was also processed under the same conditions to obtain the reference material.

Dog-bone specimens for tensile tests (type 1AB), as well as specimens for flexural tests (ISO 178), were fabricated by injection molding in a JSW 85 EL II injection machine (JSW Plastics Machinery Inc., USA) provided with a 35 mm diameter reciprocating screw. The composite pellets were dried at 150°C for 3 hours prior to processing. The processing temperature was of 360ºC, and injection was performed in a specific mold made of 1.2790 tool steel at 180°C. The screw speed was of 120 rpm, with an injection time of 0.36 s, a compaction pressure of 1000 bar and a cooling time of 3 s.

2.3. Raman spectroscopy

Spectra were measured on the surface of tensile-test specimens using a HORIBA Jobin Yvon spectrometer HR 800UV. The measuring parameters were set as follows: laser wavelength = 785 nm, hole = 500 μm, grating = 600 lines/mm, exposition = 5 s, accumulation = 5 acquisitions. The incident power was 1 mW for the PEEK specimen and 3 mW for the composites. Five spectra were measured at different random positions on each sample, and the averaged spectra are presented here.

2.4. X-Ray diffraction

Wide angle X-ray diffraction (WAXD) was performed using a PANalytical Empyrean instrument operated in the reflection mode with Bragg-Brentano geometry ($\theta - 2\theta$ mode) and equipped with a Cu K_α X-ray tube and a PIXcel 1D detector. Typically, a 2θ range of 4-40º was obtained in 1 hour experiments with a scan step of $2\theta = 0.026$º.

2.5. Thermal characterization

A Q2000 TA differential scanning calorimeter (DSC, TA instruments, USA) was used to characterize the glass transition heat capacity jump (ΔC_p), the glass transition temperature (T_g) corresponding to the heat capacity half-step temperature, and the melting (T_m), cold

crystallization (T_{cc}) and crystallization (T_c) transition temperatures from the maximum of the respective heat flow peaks. Samples of around 30 mg were extracted from tensile test specimens by die cutting. A scanning rate of 10 ºC/min was used. Calibration in temperature and enthalpy was performed using a standard indium sample. Characteristic temperatures, as well as crystalline and amorphous contents were obtained using the first heating scan, from room temperature up to 390ºC, which reflects the previous thermal history of the original sample. After 10 min at 390ºC, a cooling scan was performed to determine the crystallization temperature and its enthalpy content. A heat of fusion for a 100% crystalline PEEK sample $\Delta H_{100\%}$= 130 J/g and a specific heat jump at the glass transition for a 100% amorphous PEEK sample $\Delta C_{p,100\%}$ = 0.27 J/g·K were considered for calculations [25]. It has to be mentioned that several values have been published for $\Delta C_{p,100\%}$ in the range between 0.2 and 0.35 J/g·K [26-29], which leads to an additional uncertainty when the amorphous fraction is calculated. Four samples from two tensile test specimens (one sample near to and one far from the injection point) were measured and the averaged data are here reported.

Thermal conductivity (κ) measurements were performed at 19 ± 1ºC using a TCi^{TM} thermal conductivity analyzer (C-Therm Technologies, Canada) based on the modified transient plane source technique (MTPS). Three bending-test samples were firmly clamped together in order to cover all the area of the sensor. Blotter tests, as suggested by C-Therm, indicate a negligible influence of the finite thickness of the sample (4 mm) on the results. Thermal conductivity was measured along the thickness direction of the bending test sample. Pyrex was tested as a reference sample and the value was only 0.7% lower than the accepted literature value, well within a 5% of the accuracy of the MTPS method. The effect of assembling three small pieces to form the testing sample was checked with poly(methyl methacrylate) (PMMA) and only a 5% increase was obtained in comparison with the measurement on a fully solid sample with the same thickness.

2.6. Mechanical properties

Uniaxial tensile tests were conducted according to ASTM D638M with an Instron machine model 5565 at 10 mm/min under displacement control. Nominal dimensions of tensile specimens were: constant gage length of 30 mm, width of 5 mm, and thickness of 2 mm. Specimens had a 14 mm smooth transition from the gage to the 10 mm wide shoulders. Strain in tensile tests was measured with a video-extensometer, marking two reference points at 10 mm inside the gage length. From the stress-strain (σ-ε) curves, the following mechanical parameters were obtained: Young´s modulus E, ultimate tensile strength σ_{TS}, fracture strain ε^*, and work of fracture W. Three-point bending tests on 10 x 4 x 80 mm^3 samples were also performed at 2 mm/min under displacement control, so that flexural modulus E_b and bending fracture stress σ_b were determined. Three samples of each material were measured to obtain the average value for all mentioned parameters.

Fractography analysis was conducted on cryogenic fracture surfaces, which were subsequently coated with gold using a sputtering device (Balzers SCD-4). The samples were observed with a scanning electron microscope (SEM, Jeol JSM-6400) in the secondary electron mode at 15 keV, with 15 mm of working distance, and a probe current of $6 \cdot 10^{-10}$ A.

Vickers hardness was measured on planar samples with a microhardness tester (Matsuzawa Digital Microhardness Tester MXT70, Matsuzawa Co., Akita, Japan). A standard Vickers indenter was utilized, with a load of 200 g and an indentation loading time of 15 s. An average value of at least three measurements and their standard deviation is presented in this work for one specimen of each GNPx/PEEK composite produced by injection molding.

2.7. Tribology behavior

Tribological measurements were carried out by means of a commercial ball-on-disk tribometer (CSM instruments, Peseux, Switzerland). The equipment is provided with a rotating vessel, which contained the sample plates (3 x 10 x 10 mm^3 and average roughness R_a = 1 μm). The counterpart was a stationary ball made of alumina (6 mm in diameter, R_a = 0.05 ± 0.002 μm). The lubricant was deionized water and the environment temperature was set to 37 ± 0.5 ºC. The applied load was 5 N, resulting in a hertzian contact pressure of 37 MPa, which is in the range of peak contact stresses for some polyethylene components in total knee replacements [30]. The diameter of the circular track was 4 mm and the sliding speed 0.05 m/s. The coefficient of friction was monitored in three sample plates for each GNPx/PEEK material during 2, 24 and 48 hours, which correspond to sliding distances of 180, 2160 and 4520 m. The wear rate (k) was calculated in the same samples after 24 h and 48 h, since the 2 h experiment did not generate any discernible track. The k value was calculated from the expression $k = V_m/F \cdot s$, where F is the perpendicular applied load, s the sliding distance and V_m the worn volume. The V_m was calculated from the wear track radius r and the average worn area A_m through the relationship $V_m = 2\pi r A_m$. The area is an average of four track profiles, which were obtained in two diametrically opposite lines on the plates using a confocal microscope Sensofar PLu 2300 optical imaging profiler (Sensofar, Barcelona, Spain).

3. Results and discussion

3.1. Raman spectra

It is well-known that Raman measurements on PEEK have to be performed using low-energy lasers, since high-energy lasers cause a strong fluorescence [31]. Many of the PEEK spectra available in the literature have been measured with a near infrared laser at 1064 nm [31-35]. In the present work, PEEK was measured with a red laser at 785 nm. In

spite of applying a very low incident power, PEEK produced substantial fluorescence with a background increasing towards low Raman frequencies. The presence of GNPs in the PEEK composites progressively decreased the background fluorescence with increasing GNP percentages (results not shown), which might be due to fluorescence quenching in graphene.

Background-subtracted Raman spectra, normalized to the most intense peak in each case, are shown in Figure 1. The spectrum of neat PEEK is rather noisy due to the effect of fluorescence, while the noise progressively decreases for composites with increasing GNP amounts. Various characteristic peaks of PEEK can be seen in the spectra of all the composites: i) the out-of-plane C-H deformation of phenylene rings at around 808 cm^{-1} [35]; ii) a complex band at around 1145 cm^{-1} including C-CO-C skeletal vibrations, ring stretching modes and C-O modes [31]; and iii) features associated to C=O and C=C stretching vibrations in the range of 1550 to 1700 cm^{-1} [31]. The peak couples at around 1595/1607 cm^{-1} and 1644/1651 cm^{-1} have been associated to the polymer crystallinity, as it will be mentioned in Section 3.3.

The GNP spectrum (Figure 1) shows the usual features of graphene materials, including the G band at 1580 cm^{-1}, the D band at 1350 cm^{-1}, and the 2D band at around 2700 cm^{-1}. The D band can be observed only in some of the composites (GNP5/PEEK), while the 2D band does not appear in any of the composites. The presence of the polymer seems to hinder the D and 2D band resonance. The effect might be tentatively associated to PEEK fluorescence. The G band can be observed in the GNPx/PEEK composites, overlapped with the PEEK signal at 1595 cm^{-1}, with an increasing intensity for increasing graphene amounts. Therefore, the G line can be used as a verification of the composite composition.

3.2. X-Ray diffraction measurements

WAXD patterns for the neat PEEK and the GNP10/PEEK composite are shown in Figure 2. In both cases, peaks are detected at 2θ = 18.61º, 20.53º, 22.45º and 28.62º, corresponding to the (110), (111), (200) and (211)+(202) reflections of orthorhombic PEEK. From the angular position of the reflections, the unit cell dimensions can be estimated [36] as a = 0.791 nm, b = 0.596 nm and c = 1.03 nm, in agreement with literature values [37]. The results indicate that the GNP filler has no influence in the cell parameters of the PEEK matrix.

The average crystallite size d can be estimated using the Scherrer equation. From the (220) reflection, the d value for the GNP10/PEEK composite (8.3 nm) is only 10% lower than for the neat PEEK (9.2 nm), indicating a weak effect of GNPs on the lamellar size. In the case of the GNP10/PEEK composite a large reflection appears at 26.47º corresponding to the graphitic peak of GNPs [38].

Assuming a two phase (crystalline and amorphous) model for PEEK, the crystalline fraction can be evaluated. In order to simulate the broad halo coming from a fully amorphous sample, different model backgrounds from the literature were tried [39-41]. In Figure 2, one of the plausible backgrounds is represented. With this approximate calculation method, a crystalline fraction of 45-47% is estimated, clearly indicating that a large amorphous content (53-55%) is present in the neat PEEK and in PEEK/GNP composites as well. In the next section, the nature of the amorphous phase will be further discussed using DSC data.

A significant change in the relative intensities of the (110) and (200) reflections is revealed in Figure 2 when the neat PEEK and the GNP10/PEEK composite are compared. An analogous behaviour has been reported by Tewatia et al. [23] in melt-blended

graphene/PEEK composites. The effect is probably associated to the preferential orientation of some PEEK crystals, which is induced by the presence of the GNP filler and is related to surface crystallization (transcrystallinity) on GNPs [42].

3.3. Thermal properties

In Figure 3, the first heating and cooling DSC thermograms are represented for the unfilled PEEK and the GNP/PEEK composites. Average values from the complete DSC data set are reported in Table 1.

In the first heating (Figure 3a) all the samples present a glass transition at 140-150ºC, followed by a small exothermic cold crystallization peak at $T_{cc} \approx$ 160-165ºC, and finally an endothermic melting transition at high temperature. The melting temperature T_m does not change significantly with the GNP weight fraction, being in the range of T_m = 347.6-348.0ºC. Additionally, small anomalies exist below the melting peak, but above the cold crystallization, for some of the samples. These anomalies are probably related to the presence of imperfect crystals, formed during the manufacturing process. The degree of crystallinity can be obtained as $x_c = (\Delta H_m - \Delta H_{cc})/(y \cdot \Delta H_{100\%})$ where ΔH_m and ΔH_{cc} are the enthalpy contents of the melting peak and the cold crystallization respectively and *y* is the weight fraction of PEEK in the corresponding composite (Table 1, Figure 4a). DSC experiments highlight that the addition of GNPs up to 10 wt. % does not largely alter the amount of PEEK crystalline phase (Figure 4a) since the estimated value of x_c for the pure PEEK sample is 39 ± 3 % and the values for the composite samples lie between 34 - 37%. In the calculation, the cold crystallization for each sample is taken into account, but it is almost negligible (ΔH_{cc} < 1 J/g). The calculated crystallinity is in good agreement with that obtained from WAXD data (Section 3.2). The lowest amount of crystalline phase, 34.2 ± 0.7 % corresponds to the GNP3/PEEK composite and increases again for higher GNP concentrations (Figure 4a). This trend is in agreement with the Raman intensity

ratios of the signal pairs at 1597-1607 cm^{-1} and 1646-1651 cm^{-1} in the C=O and C=C stretching region of PEEK (Figure 4b), which have been previously related to PEEK crystallinity [31].

Cooling DSC curves (Figure 3b) show peak crystallization temperatures T_c that increase from 308.9 ± 0.1 ºC for pristine PEEK up to 313.2 ºC ± 0.3 ºC as the GNP fraction increases, with the steepest variation for GNP1/PEEK (Table 1 and Figure 3b). However, the crystallization enthalpy content ΔH_c does not show any clear trend and can be considered almost independent of the GNP content (54 ± 3 J/g). Such an enthalpy value corresponds to a x_c = 39-44%, which is larger than that determined from melting peaks. Actually, the DSC cooling process is not representative of the thermal history undergone by the melt during injection.

From DSC cooling, it is interesting to note that the presence of GNPs provides surfaces for heterogeneous nucleation. In fact, crystallisation peaks start at higher temperatures as the GNP content increases, indicating some transcrystallinity (unidirectional crystal growth perpendicular to the surface of the GNP layers). However, the transcrystalline region apparently has small contributions to the enthalpy and the total crystalline fraction. After nucleation, at least two phenomena might prevent the growth of crystals on GNPs: i) the mobility of polymeric chains might be hindered by the presence of GNPs, and ii) the nucleation and growth of spherulites in the bulk polymer might be predominant under the DSC cooling conditions, blocking the growth on GNP surfaces. Regarding the actual state after the injection process, some indication of transcrystallinity was inferred from WAXD patterns in Section 3.2.

The presence of an amorphous phase is clearly detected in both the heating and the cooling, since specific heat steps appear around 140ºC due to the glass transition. On

heating, T_g does not follow any trend with the GNP content, being $T_{g,heat}$ = 139-143ºC. Thus, the filler does not reduce the segmental mobility of the polymer chains. In the cooling scan from the melt, $T_{g,cool}$ is 146.1 ± 0.4 ºC for the unfilled PEEK and a small decrease of around 2-3ºC is obtained with the presence of GNPs. In addition, $T_{g,,cool}$ values are 2ºC higher than those from the first heating. These results confirm a lubricant effect of GNP fillers [43, 44]. It must be pointed out that neither T_g nor ΔC_p of the unfilled PEEK can be accurately evaluated due to an anomalous behavior in the 120-140ºC temperature range consisting of a small endothermic feature followed by a small exothermic anomaly (Figure 3a). It has been reported that such anomalies are associated to internal stresses in glasses obtained by cooling from a pressure-densified melt [45]. Both anomalies decrease for the composite samples, indicating that the presence of GNPs favors the reduction of residual stresses and the physical ageing of the amorphous phase.

The specific heat step at the glass transition ΔC_p for all the samples is small (< 0.1 J/g·K) and it can be only determined with a large uncertainty. If the 53-55% of amorphous phase content from WAXD (Section 3.2) contributed to the glass transition, the expected ΔC_p would be around 0.14-0.15 J/g·K. Since the experimental ΔC_p is clearly lower than that, not all the amorphous phase contributes to the glass transition, suggesting a more complex polymer structure.

The previously mentioned uncertainty prevents a precise estimation of the amorphous phase content using $x_a = \Delta C_p/(y \cdot \Delta C_{p,100\%})$ and therefore only a rough value of x_a = 31-33% can be calculated. It is evident that the sum of the crystalline and amorphous fractions does not reach 100%, invalidating the two-phase model. Depending of their thermo-mechanical history, PEEK and other semicrystalline polymers contain a third component, called the rigid amorphous phase, which is structurally amorphous and is formed by portions of entangled chains with a hindered mobility due to the proximity of

crystalline structures [25, 46]. It has been reported that the rigid amorphous phase does not contribute neither to the heat of fusion nor to the heat capacity step at the glass transition [25, 47], and that the rigid amorphous phase in PEEK relaxes little by little as the temperature increases above the glass transition [48]. Therefore, the previously calculated x_a corresponds to the mobile amorphous fraction x_{ma}, and the rigid amorphous fraction x_{ra} can be calculated as $x_{ra} = 1-x_c-x_{ma}$, roughly being a 31-33% for all the samples. Consequently, GNPs does not seem to provide significantly additional effective surfaces to favor the immobilization of polymeric chains. Even though the previously determined variation in x_c (Figure 4a) must be related with changes in the amorphous phase fractions, the uncertainty in ΔC_p does not allow to distinguish if it corresponds to the mobile, the rigid or both amorphous components.

The thermal conductivity κ for the blank PEEK material resulted to be 0.53 ± 0.02 W/m·K. The value is higher than those previously reported for PEEK samples with a similar crystalline content (0.25-0.31 W/m·K) [49, 50], and lower than that measured in a mechanically drawn (oriented) specimen (0.59 W/m·K) [51]. The processing conditions, which may induce different crystalline orientations can be behind the κ variations.

The values of κ and x_c are jointly depicted in Figure 4a as a function of the GNP content, both showing a similar trend. The addition of GNPs up to 3 wt. % slightly reduces κ down to 0.44 W/m·K, and then κ increases again for higher concentrations. Theoretically, a significant improvement in κ should be expected as the GNP content increases since the thermal conductivity of graphene has been estimated to be around 5000 W/m·K [52]. In addition, considerable thermal conductivity improvements between 20 - 70% have been reported for different polymer matrices (epoxy, PBT, PPS, silicone, PE, PP, PVA and PVDF) using graphene fillers [53]. So far there are not literature works reporting the thermal conductivity of PEEK composites with bare GNP fillers, and only

two articles include κ data for GO/PEEK composites and graphene/carbon fiber/PEEK laminates [54, 55]. In the case of GO/PEEK composites, a thermal conductivity improvement of 100% was achieved, although the κ value of 0.18 W/m·K for of the unfilled PEEK was very low considering the high $x_c = 0.58$ [54]. In the other reference, a commercial graphene material was added to carbon fiber/PEEK laminates and κ increased by 54% for 1 wt. % graphene [55].

According to Li et al. [53], several factors might cause the κ decrease observed at low GNP percentages in the present work. First, a completely homogeneous distribution of the filler at the microscale might be difficult during injection molding. Second, filler-polymer and filler-filler interfacial interactions might be a source of phonon scattering. Third, the decrease in the degree of crystallinity, as it is shown in Figure 4, might contribute to the degradation of heat transfer through the composite. On the other hand, certain recent works follow a different strategy for improving κ, based on the formation of a segregated conductive network instead of the simple filler dispersion [56, 57]. In the present work, the conductive network starts to be active at high GNP concentrations (5 and 10 wt. %), overcoming the negative effects due to changes in the polymer morphology.

3.3. Mechanical properties

The tensile σ-ε curve for the blank PEEK specimen (Figure 5a) shows the standard shape of a PEEK material. After the initial region with a Young's modulus of 3.61 ± 0.08 GPa, the polymer yields at a stress of 105.6 ± 1.9 MPa, following with a neck-formed region, a short neck propagation at a constant stress with no strain harden, and the final fracture at a strain of 21 %. The test parameters are in agreement with the literature: 1.02-4.1 GPa for the modulus, 80-124 MPa for the tensile strength and 5-95 % for the fracture strain [9, 58-

60]. In GNPx/PEEK composites, σ-ε curves (Figure 5a) show a positive correlation between the GNP wt. % and the Young`s modulus, reaching a value of 5.34 ± 1.9 GPa with 10 wt% of filler, which corresponds to an increase of 48 % in stiffness. Tensile strength stress slightly decreases down to 87.5 ± 4.2 MPa for GNP10/PEEK (Figure 5a). Moreover, the introduction of GNPs produced a strong decrease in the elongation at break, which drastically affects the toughness (work of fracture). Table 2 summarizes all the parameters deduced from the tensile curves. The 3-point bending test for the blank PEEK (Figure 5b) gives a flexural modulus of 3.11 ± 0.19 GPa and a flexural strength of 166.2 ± 2.4 MPa, in accordance to previous published works [23]. The influence of the GNP filler is analogous to tensile outcomes, with an increase of 17 % in the modulus until reaching 3.76 ± 0.22 GPa for the GNP10/PEEK composite. Flexural curves (Figure 5b) point out that flexural strength also undergoes a slight reduction, while a drop in the flexural deformation and toughness appears, as it is reflected in Table 3.

The strong increase observed in the stiffness of PEEK with the incorporation of GNP fillers cannot be attributed to changes occurring in the matrix microstructure. The degree of crystallinity, which directly influences the modulus of semicrystalline polymers, does not exceed the PEEK value of 39 ± 3 % in any of the composites. The rigid amorphous fraction, which could contribute to the stiffness [61], also remains constant at around 31-33%. Therefore, the increase in the Young's modulus with respect to the unfilled PEEK is clearly related to the intrinsic modulus of graphene and its high aspect ratio, which provides large interfaces with the matrix. In addition, trancrystallinity might provide an increase in the filler/matrix adhesion. The effect has been also observed in other polymeric systems, for instance in UHMWPE [19].

The reduction in yield stress after the addition of GNP fillers might be associated to a decrease in the lamellae thickness L_c. However, the melting temperature does not

change and both T_m and L_c are correlated through the Gibbs-Thomson equation: $T_m = T_{m,100\%} (1-2\sigma_s/L_c\rho_c\Delta H_{m,100\%})$, where σ_s is the specific surface energy, ρ_c is the density of the crystalline phase, and $\Delta H_{m,100\%}$ is the melting enthalpy of a perfect crystalline polymer. It has also been shown that the presence of a rigid amorphous phase in semi-crystalline polymers might lower the yield stress and produce embrittlement [47, 62]. However, the effect seems to be irrelevant in our GNPx/PEEK series, since the fractions of the three phases (crystalline, rigid amorphous and mobile amorphous) remain almost constant with the GNP content. Since tensile strength is approximately constant with respect to GNP concentration, the embrittlement induced by GNPs is probably connected with a loss in ductility.

Plastic mechanisms associated with crystalline deformation via rotation, shearing and fragmentation of lamellae, and with viscous flow in the amorphous phase, are the causes of permanent deformations in pure PEEK [39, 63]. Yang et al. [59] prepared PEEK composites of thermally reduced GO and found a 90 % reduction in the tensile toughness at 5 wt. % of filler, which is a higher reduction than in the present work. Recently, Tewatia et al. [23] utilized graphene flakes with 2-6 layers and reported flexural σ-ε curves for 0, 2 and 5 wt. % of graphene. The curves practically overlapped at flexural strains of 5 wt. %, which was set as the deformation limit in the bending test. Evidently at that strain the composites did not reach fracture. Other attempts using different carbonaceous fillers such as carbon nanotubes gave similar results [58].

In the literature, the decrease in the work of fracture has been associated to the presence of filler aggregates that act as stress raisers and lead to an early fracture. In order to detect possible GNP aggregates, SEM images of cryogenic fracture surfaces were carried out on neat PEEK and GNPx/PEEK composites. Figure 6a-e shows fractographies at a low magnification, which would be suitable to detect the aggregates, if they existed.

The other pictures in Figure 6 were taken at higher magnifications. The unfilled PEEK (Figures 6a and 6f) shows a squamous-like morphology due to its brittleness at cryogenic temperatures. For the GNP1/PEEK composite (Figures 6b and 6g), the fracture surface is smoother than in pure PEEK, in accordance with the decrease in toughness at room temperature. However, the presence of GNPs or GNP aggregates is not evidenced in any of the images at low GNP loadings. Other morphologies appear at the highest GNP percentages (Figures 6d and 6e). At 5-10 wt.% of GNPs, the materials exhibit rough surfaces, some cracks and other additional curve elements. The high magnification images (Figure 6i and 6j) show stacked graphene sheets, although their dimensions do not achieve the initial specifications from the supplier. The fractographies indicate that the formation of GNP aggregates is not the cause for the loss of toughness in the composites, since at the lowest graphene concentrations there in not any evidence of aggregates and the reduction in the deformation to fracture is already ~ 50 % for the GNP1/PEEK composite. This behavior has been also mentioned by Mittal et al. [64] comparing the mechanical properties of various graphene-reinforced polymers. Therefore, the presence of GNPs affects the deformation of fracture through a decrease in the number of deformation modes, even at the lowest graphene loadings.

Concurrently, the incorporation of GNPs into PEEK produced a relevant increase in hardness, according to data shown in Figure 7. At the highest GNP concentrations, the micro-hardness reaches 310 $HV_{0.2}$ (MPa), which is a 29% of increase with respect to the neat PEEK. The increase in hardness is progressive upon the addition of GNPs. The hardness increment could be associated to graphene-matrix interactions that prevent plastic deformation in the matrix. The trend has been confirmed by experimental results in another graphene/polymer system [65], and also by a recent molecular simulation for graphene/polymer composites that predicts a 35% decrease in the indentation depth [66].

The reorganization of amorphous polymer chains in the surroundings of graphene nanoparticles produces a higher resistance against the normal loading applied by the indenter. However, the positive influence of GNPs in PEEK hardness does not appear in Kalin et al. [20], which observed a reduction of 20-25% for a composite with 2 wt. % of GNPs.

3.5. Frictional behavior

The plot of the coefficient of friction (COF) vs. the sliding distance reaches, after the running regime, a plateau for all the samples. Figure 8a shows COF curves for the initial 2 h period, averaging 3 measurements per sample. The steady-state value in unfilled PEEK is about 0.13 ± 0.02, in agreement with the value of 0.14 obtained by Unal. et al [67] under water lubrication, the same sliding time, but a different tribometer counterpart (AISI D2 steel). It is also close to the value of 0.155 reported by Song et al. [21] with a steel tribometer ball and a relative humidity of 40-60%. Figure 8a shows the positive influence of GNP addition on friction. The values of COF at the stationary regime for the different composites are: 0.11 ± 0.03, 0.10 ± 0.02, 0.10 ± 0.03 and 0.08 ± 0.02 for the 1, 3, 5 and 10 wt. % of GNP composites, respectively. Although the reduction in friction with the presence of GNPs is observed in the long-term test too (Figure 8b), a correlation between COF and the amount of GNPs is not so clear. A minimum COF value of 0.1 was obtained for GNP3/PEEK, and the other composites present values below 0.16, which is the COF for the neat PEEK after 48 hours of testing.

The COF results confirm the lubrication capability of graphene in polymer composites, which has been recently estimated by Li et al. [66] using molecular dynamics simulations. On the other hand, the fact of using multilayer graphene particles (around 30

layers in this case) also contributes to improve the single sheet lubricant properties, according to simulations by Kim et al. [68] and atomic force microscopy experiments by Kaway et al. [69]. In both cases, they found that friction depends on the number of layers in the graphene flakes, with a decreased friction for the multi-layer system. The best interlayer sliding and the lowest out-of-plane elastic deformation takes place in multilayer graphene particles. Similar results about the positive influence of the graphene particle thickness on the COF have been obtained by Bhargava et al. in PTFE composites [18].

The lubricating effect of graphene in polymer composites has been previously shown for the particular case of PEEK. Song et al. [21] obtained a reduction from 0.16 to 0.10 with a GO filler content of 1.0 wt. %, although the results were deduced from a test of 20 minutes, which is a very short-term experiment. Other graphene fillers similar to the GNP of the present study were utilized by Kalin et al. [20] and Liu et al. [55]. In the present work, 1 wt. % is enough to improve the frictional behavior with respect to the unfilled PEEK. In carbon fiber/PEEK laminates, Liu et al. [55] observed that 0.7 wt. % of graphene produced a reduction in the COF from 0.48 to 0.37.

3.6. Wear resistance

Confocal and SEM microscopy images of the worn surfaces were carried out for the unfilled PEEK and the composites after sliding times of 24 and 48 h. In Figure 9a, obtained by confocal microscopy, a circular track of 0.6 mm width is presented. The image corresponds to PEEK after 48 h of wear process, and exhibits grooves parallel to the sliding direction with wear scratches of around 25 μm. Figure 9b plots various profiles, after 48 h of sliding contact, for PEEK and GNPx/PEEK composites.

Figure 9c shows the resulting values of k for PEEK and the GNPx/PEEK composites. The wear rate for unfilled PEEK was $22 \cdot 10^{-7}$ $mm^3/N \cdot m$, in the same order of

magnitude as the average value of $50 \cdot 10^{-7}$ $mm^3/N \cdot m$ obtained by Jacobs et al. using a ball-on-prism tribometer with similar conditions of lubrication and counterpart material [70]. The wear volume follows a linear relationship with the distance for all the GNPx/PEEK materials, since k is practically equal at 24 h and 48 h of sliding. The trend was reflected in all the measurements, except for GNP3/PEEK after 48 h of sliding, which resulted to be at the level of neat PEEK without any plausible explanation. The most relevant result deduced from Figure 9c is the positive influence of GNP on the wear resistance. The higher the concentration of the filler, the lower the wear factor is, reaching values close to $4 \cdot 10^{-7}$ $mm^3/N \cdot m$ in GNP10/PEEK, five times lower than the neat PEEK. In order to explain the mechanisms involved in the wear process, worn surfaces as well as the Al_2O_3 ball counterpart surfaces were analyzed by SEM.

Figure 10a shows SEM images of the unfilled PEEK after 48 h of wear process at low magnifications. The images reveal grooves parallel to the sliding direction and unevenly eroded patches that can be associated to mechanisms of adhesion and abrasion wear. The scratches make evident the involvement of plastic deformation, which is also reflected by the edges of some of the patches at higher magnifications (Figure 10b). The morphology clearly contrasts with that obtained in zones far from the wear track, where a clumpy structure appears (Figure 10c).

The combination of adhesion and abrasion has been previously observed using other bearing pairs, such as PEEK-steel in a relative humidity of 40-60 % [21], and a dry-sliding contact [20]. More specifically, the proposed mechanism was based on the formation of scales in the wide scratches, followed by a transfer to the counterpart ball and the subsequent adhesion, again onto the polymer surface, in the form of films [20]. However, in the present work, probably due to water lubrication, the transfer stage does not happen and no adhered material can be observed on the ceramic counterpart. Figure

11a is an SEM image of the Al_2O_3 ball surface before the wear contact, showing the presence of some pores. After sliding against the neat PEEK (Figure 11b) and GNP10/PEEK (Figure 11c), the Al_2O_3 ball surface shows scratches but no rests of the plastic material. The behavior agrees with the idea that water lubrication prevents the formation of transfer films [70].

Figure 12 shows SEM images of the track for all the composites after wear processes of 24 h and 48 h. After 24 h of sliding, the GNP1/PEEK specimen (Figure 12a) presents a plowed up surface partially covered by film patches. This appearance is due to a combination of adhesion and abrasion wear, analogous to neat PEEK. In GNP3/PEEK (Figure 12b), the morphology evolves to a surface with some scratches and plastic fragments oriented in the track direction. The scratches progressively disappear for GNP5/PEEK (Figure 12c) and GNP10/PEEK (Figure 12d). In the GNP10/PEEK specimen, a homogeneous surface is observed, even smoother than the unworn areas, which is only broken by some local defects with plastic morphologies in their edges. The morphologies produced on the GNPx/PEEK composites surfaces after 48 h of sliding (Figures 12e-12h) follow a trend similar to that at 24 h, with an increased effect due to the high sliding-time.

Several factors might be considered in the wear of graphene-based PEEK composites: toughness, thermal conductivity, surface hardness, filler morphology and dispersion, lubricant, and so on. Liu et al. [22] explained the decrease in COF and k values of graphene-filled PEEK/SCF/PTFE on the basis of the increase in the thermal conductivity under dry-sliding conditions. In the present work, as the thermal conductivity undergoes a slight decrease with the GNP concentration and the water lubricant reduces the temperature rise in the bearing area, thermal conductivity does not seem to be a relevant parameter for wear resistance.

The GNP10/PEEK composite shows the highest hardness and a brittle character, since the toughness decreases when the GNP percentage increases. Such mechanical characteristics seem to be associated to a smooth morphology (Figure 12d,h), where no grooves are observed and the uniformity is only broken by some cracks of up to 100 μm. The combination of high hardness and low toughness favors fatigue wear as the predominant mechanism, with generation of subsurface cracks and scales. Eventually fragments run out with the water-lubricant. On the contrary, neat PEEK and GNP1/PEEK materials show higher toughness and lower hardness. The presence of cracks is negligible, while scratch lines are observable even at low magnifications, indicating that the involved mechanism is mainly abrasion wear. The SEM images of the GNP1/PEEK composite after 48 h of sliding (Figure 12e) are the most representative of a pure abrasion behavior, since they show a track surface full of parallel grooves. Film patches on the track surfaces of PEEK and GNP1/PEEK after 24h can be interpreted as a preliminary stage in the wear process that eventually concludes with the full disappearance of the initial surface layer and the formation of the set of parallel grooves associated to the abrasion mechanism. Wear behavior for GNP3/PEEK and GNP5/PEEK composites might result from their intermediate mechanical behavior in terms of hardness and toughness. Some grooves appear as a consequence of the loss in hardness compared to GNP10/PEEK. The scratches might act as stress concentration regions, which produce subsurface cracks and scales with a coalescence along the grooves (Figures 12b,c,f). Such a wear mechanism can be considered as a combined action of fatigue and abrasion.

In summary, the improvement in the PEEK wear resistance with increasing GNP concentrations seems to be associated with the increase in hardness, which delays the abrasion wear. However, the increase in hardness at the highest GNP percentages does not compensate the simultaneous loss in toughness and consequently an incipient fatigue wear

appears. Therefore, an increase in toughness would contribute to decrease even more the already low wear rates for GNP5/PEEK and GNP10/PEEK composites. Here, graphene functionalization might be a way to improve the filler-matrix adhesion, whenever the costs are acceptable and the biocompatibility for biomedical applications is not comprised. Another strategy might be also the use of a layer of the GNP/PEEK composite as a coating on pure PEEK components, as it has been recently described for other polymers [71]. The coating would offer a good wear resistance, according to the results of this work, keeping the mechanical properties of the neat PEEK component, in particular its toughness.

4. Conclusions

Composites based on a PEEK matrix with different GNP amounts from 1 to 10 wt. % are prepared by a solvent-free melt-blending process. A three-phase model is proposed, including a crystalline phase, a mobile amorphous phase and a rigid amorphous phase, with their respective fractions quite similar in the neat PEEK and the composites. GNP fillers do not practically modify the microstructural parameters obtained by DSC and the thermal conductivity of the PEEK matrix. As a consequence, the increase observed in the tensile-flexural modulus and hardness with the increase in the GNP concentration seems to be related to the intrinsic mechanical properties of graphene. However, a toughness reduction also results from the GNP dispersion in the matrix. Remarkably, GNP fillers provide a positive influence on the coefficient of friction and more specifically in the wear rate. The improvement in k is around 83 % for the GNP10/PEEK composite, and is associated to its high value of hardness. At the highest GNP percentages, the wear mechanism seems to be fatigue wear, while at the lowest GNP concentrations abrasion wear predominates. The incorporation of GNPs into PEEK in amounts around 3-5 wt. % can reduce the frictional coefficient and the wear rate without altering the elastic modulus

and strength. In order to exploit the lubrication capability of grahene at the highest concentrations, other proposed routes might be assessed, trying to maintain the toughness of the neat PEEK.

Acknowledgements

This work has been funded by the University of Zaragoza (UZ2015-TEC-04), the MINECO together with the European Regional Development Fund (ENE 2016-79282-C5-1-R), and the Government of Aragon together with the European Social Fund (DGA T-48-17R and DGA-T03-17R. Special thanks are directed to the Analysis Service of Instituto de Carboquímica, ICB-CSIC, in particular to A.I. Díaz-Megías.

FIGURE 1. Raman spectra of PEEK, GNPx/PEEK composites and GNP powder: a) baseline corrected spectra, normalized to the most intense peak, and b) insight of the C=O and C=C stretching region of PEEK.

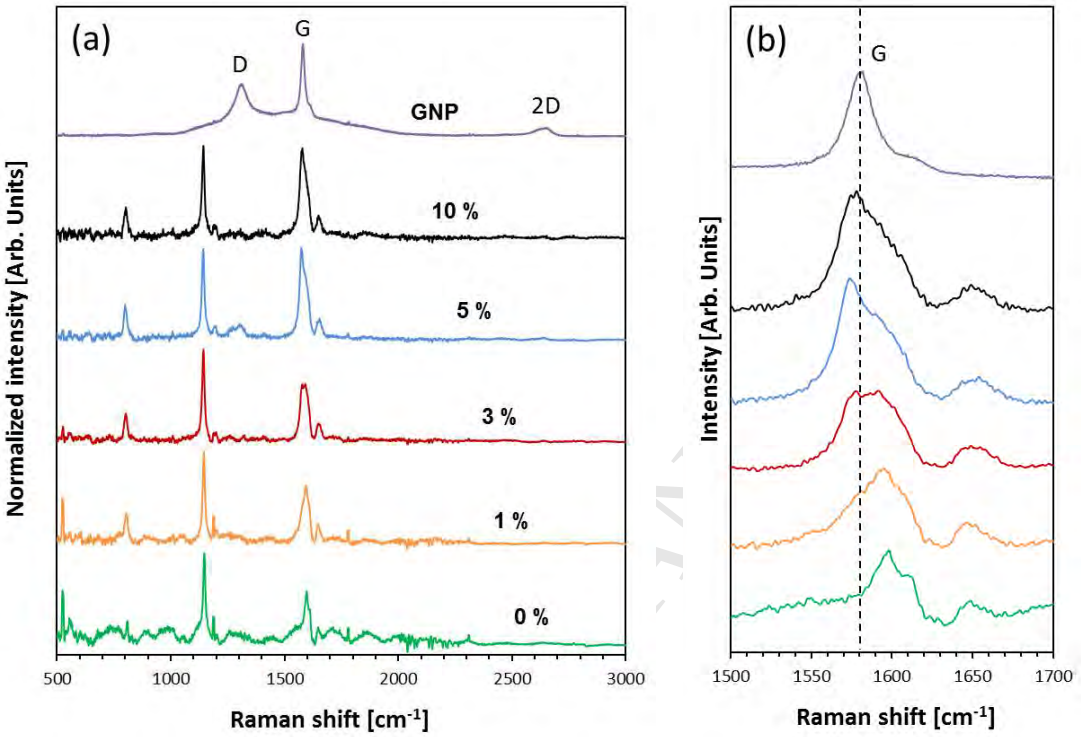

FIGURE 2. XRD patterns for the neat PEEK (green) and GNP10/PEEK (black) composite. Dashed line is a plausible background of the amorphous polymer component.

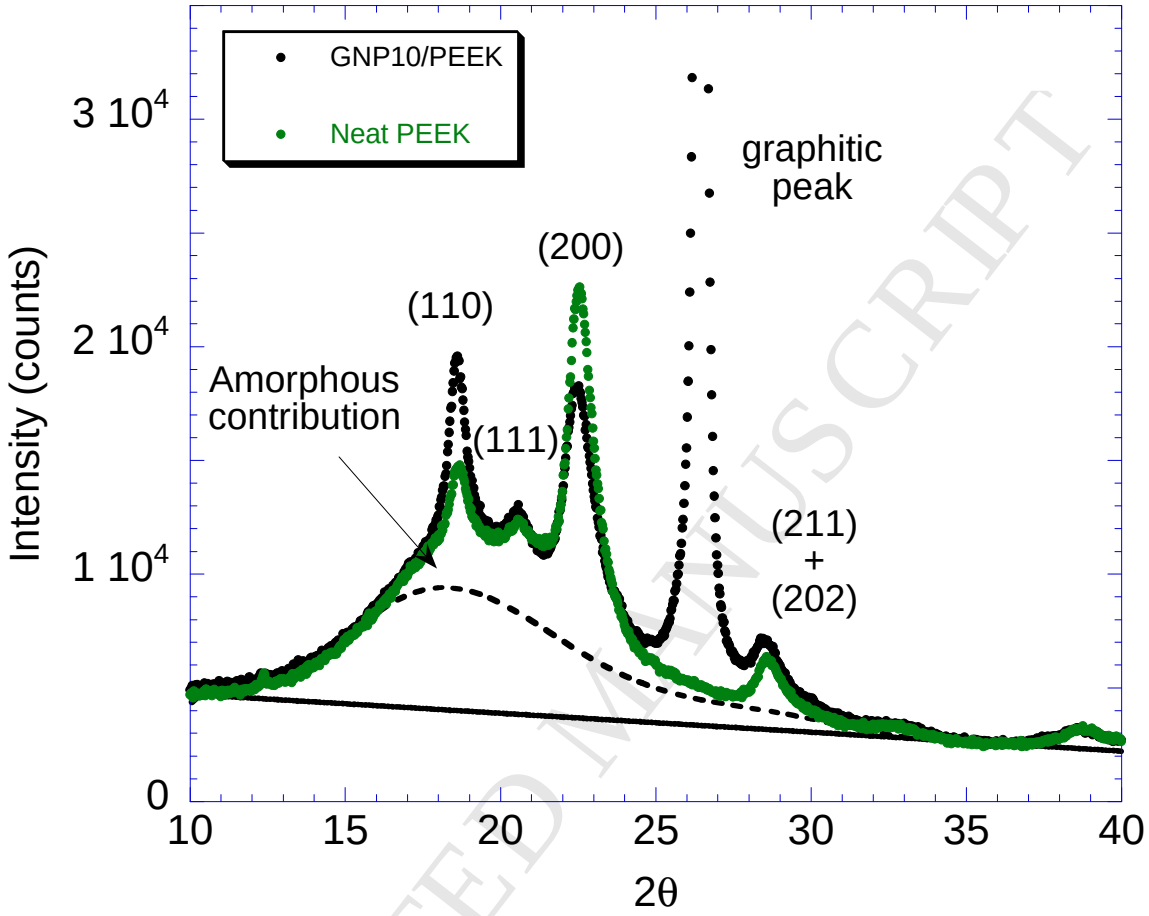

FIGURE 3. DSC thermograms for PEEK and the GNP/PEEK composites: a) first heating, and b) first cooling**.**

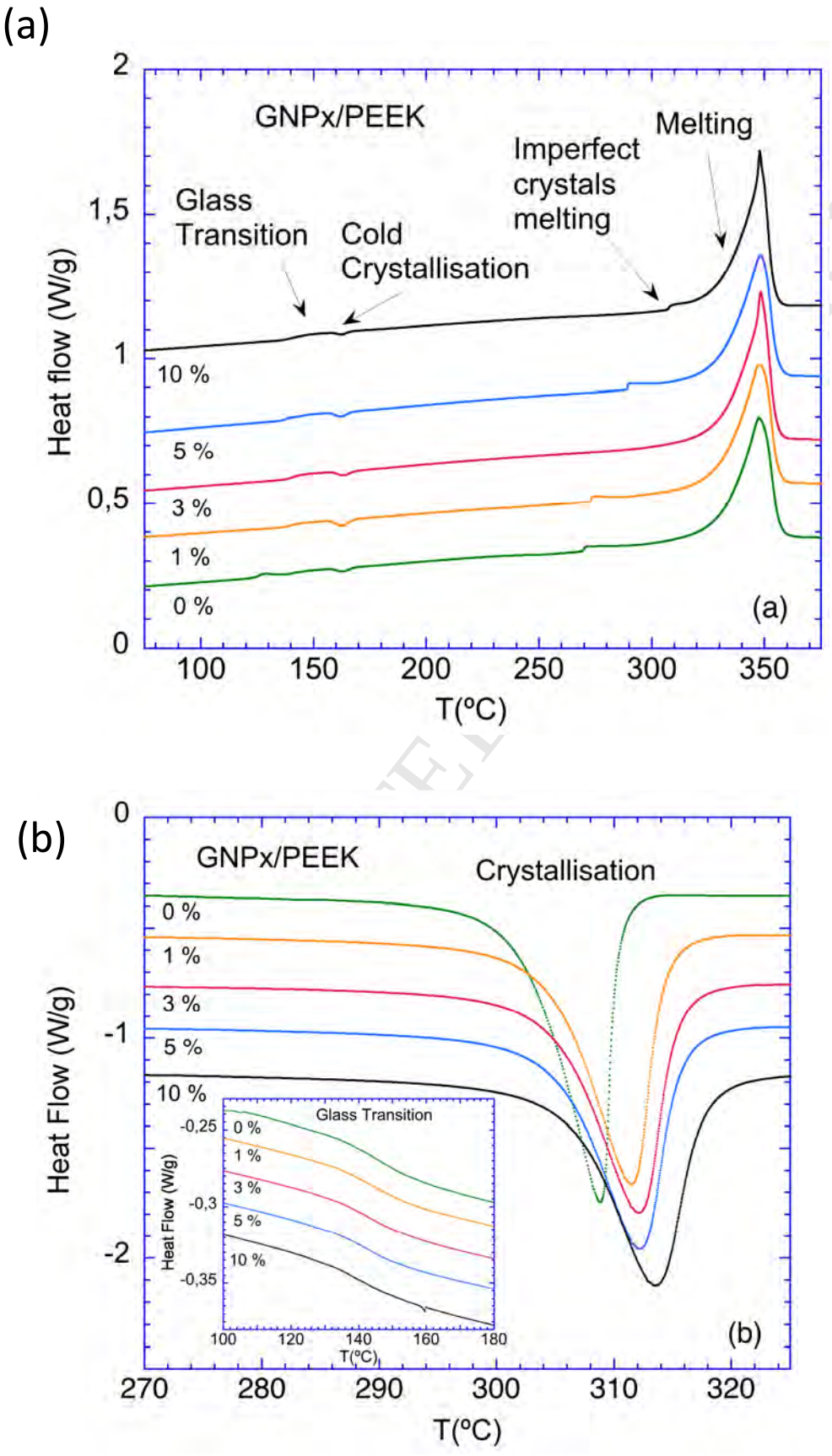

FIGURE 4. Crystallinity and thermal conductivity for PEEK and GNPx/PEEK composites: a) degree of crystallinity (x_c) from DSC and thermal conductivity (κ) vs. the GNP content (wt. %), and b) two Raman intensity ratios associated with PEEK crystallinity vs. the GNP content (wt. %).

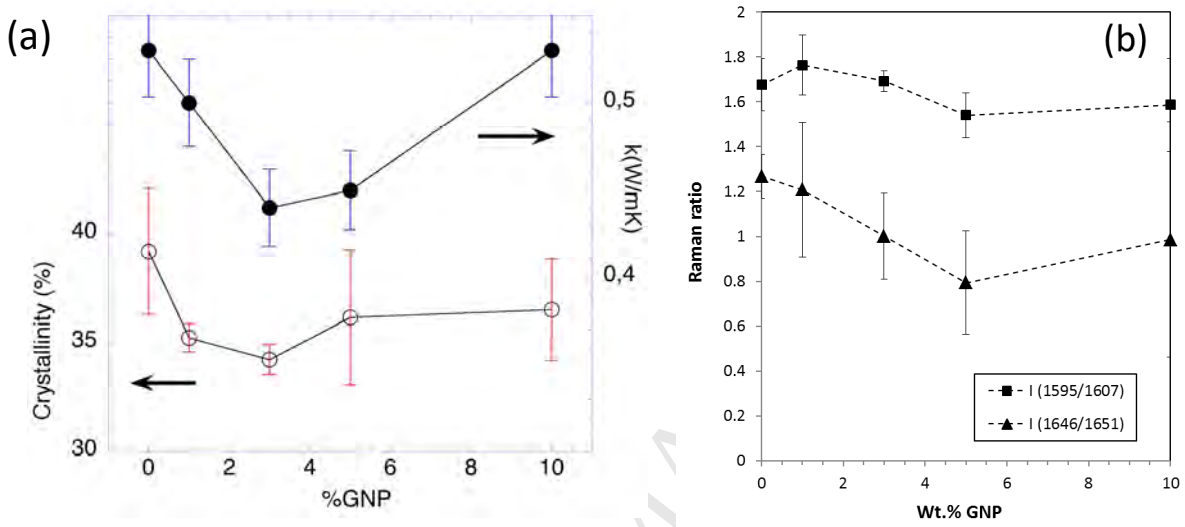

FIGURE 5. Tensile and bending measurements for PEEK and GNPx/PEEK composites: a) stress-strain curves from uniaxial tensile tests, and b) stress-displacement curves from 3-point bending tests.

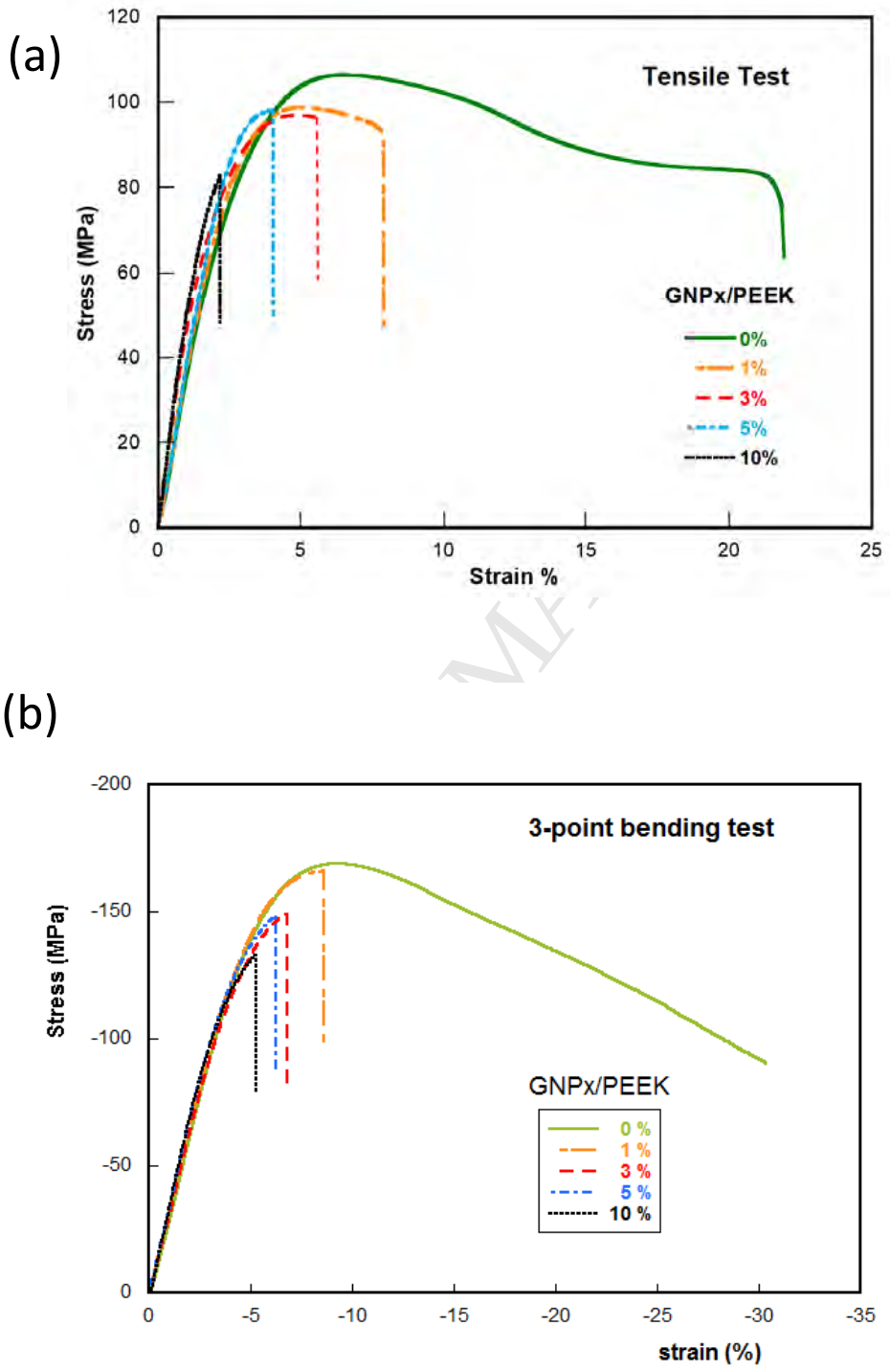

FIGURE 6. SEM images of cryogenic fracture surfaces at low magnification (a-e) and high magnification (f-m) for various samples: neat PEEK (a, f, k), GNP1/PEEK (b, g), GNP3/PEEK (c, h), GNP5/PEEK (d, i, l), and GNP10/PEEK (e, j, m).

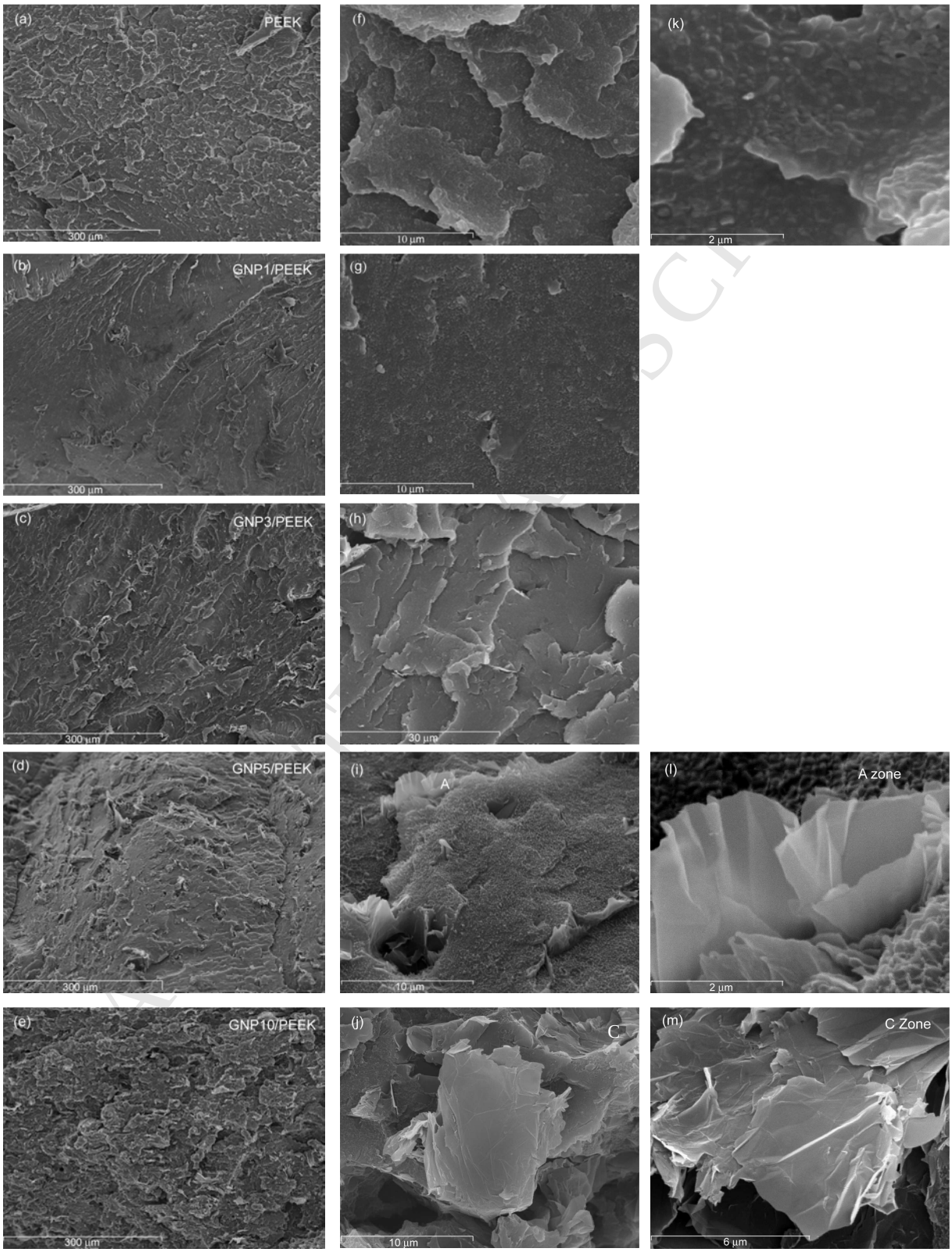

FIGURE 7. Vickers hardness vs. the GNP content (wt. %) for PEEK and GNPx/PEEK composites.

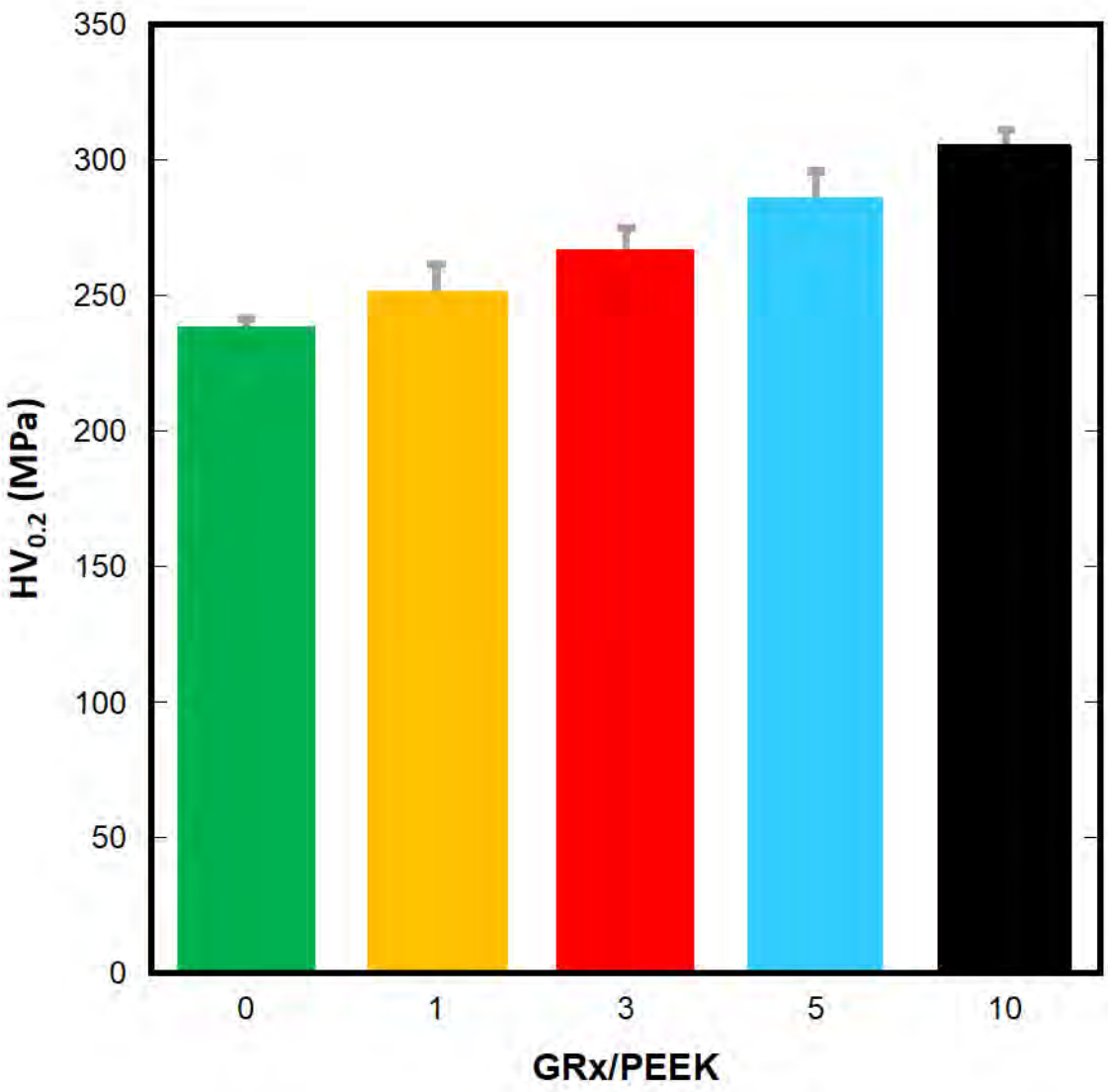

FIGURE 8. Coefficient of friction vs. sliding distance for PEEK and GNPx/PEEK composites: a) initial 2 h period (average curves of 3 experiments), and b) long term analysis (48 h).

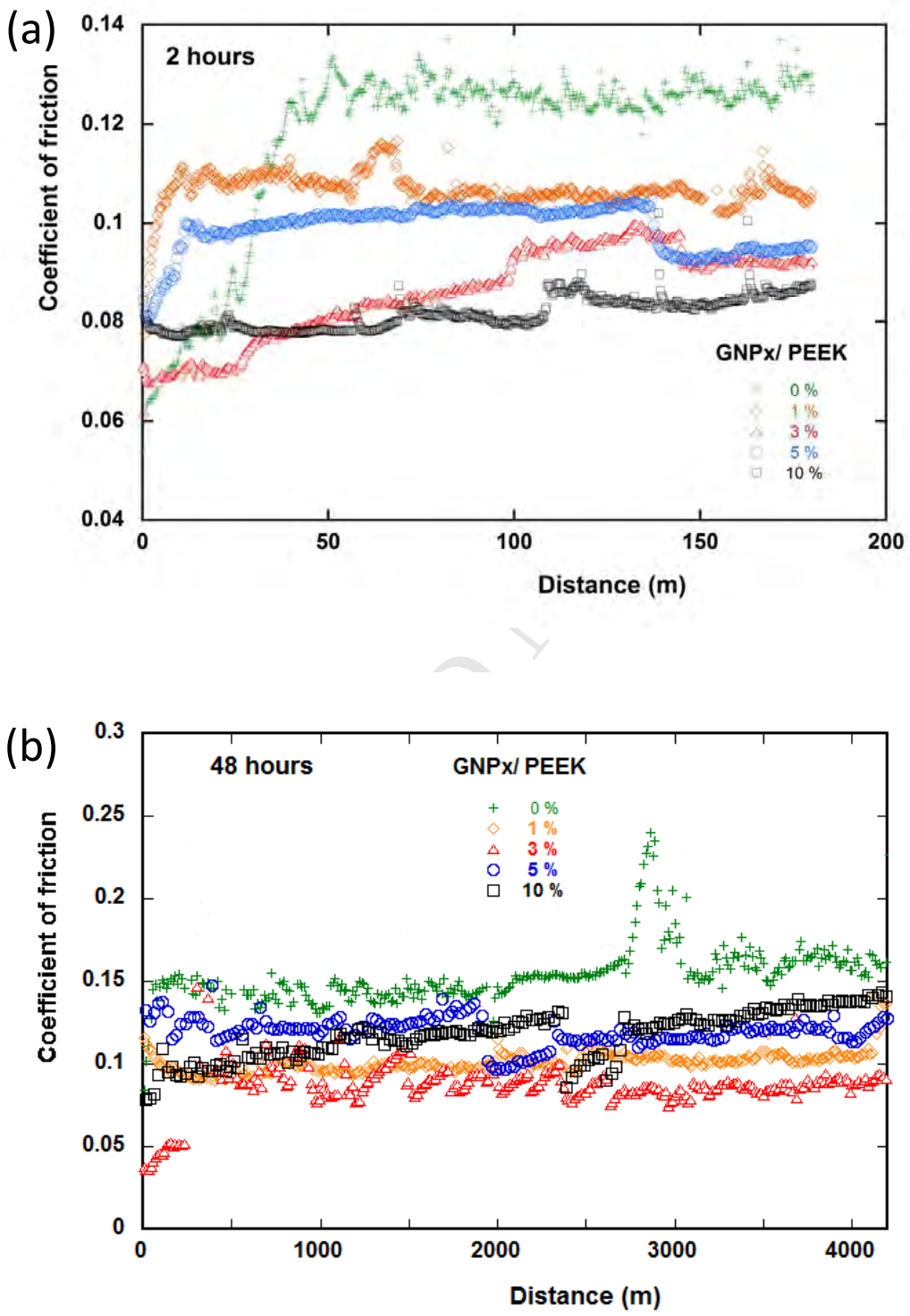

FIGURE 9. Confocal microscopy analysis of the wear process for PEEK and GNPx/PEEK composites: a) confocal image of the worn surface in neat PEEK after 48 h sliding; b) surface profiles perpendicular to the wear tracks at 48 h sliding; and c) wear rate (k) calculated from cross sectional profiles at 24 and 48 h of sliding (the dashed line is an exponential fitting of average values at each GNP percentage).

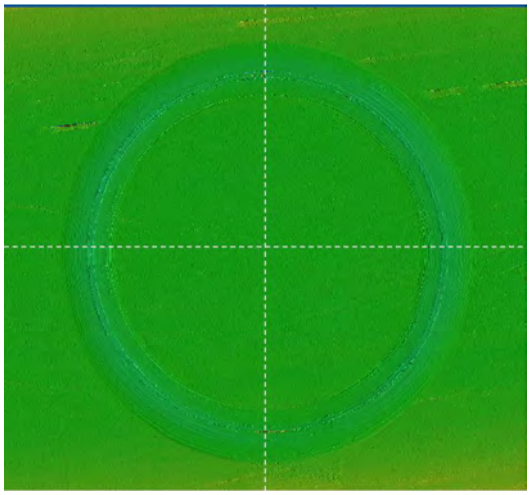

(a)

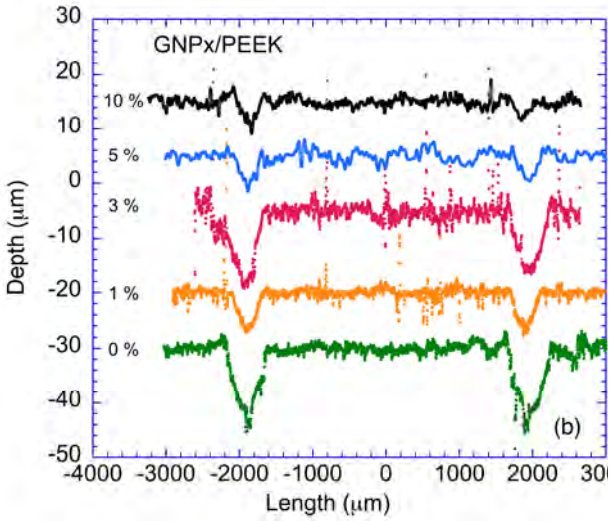

(b)

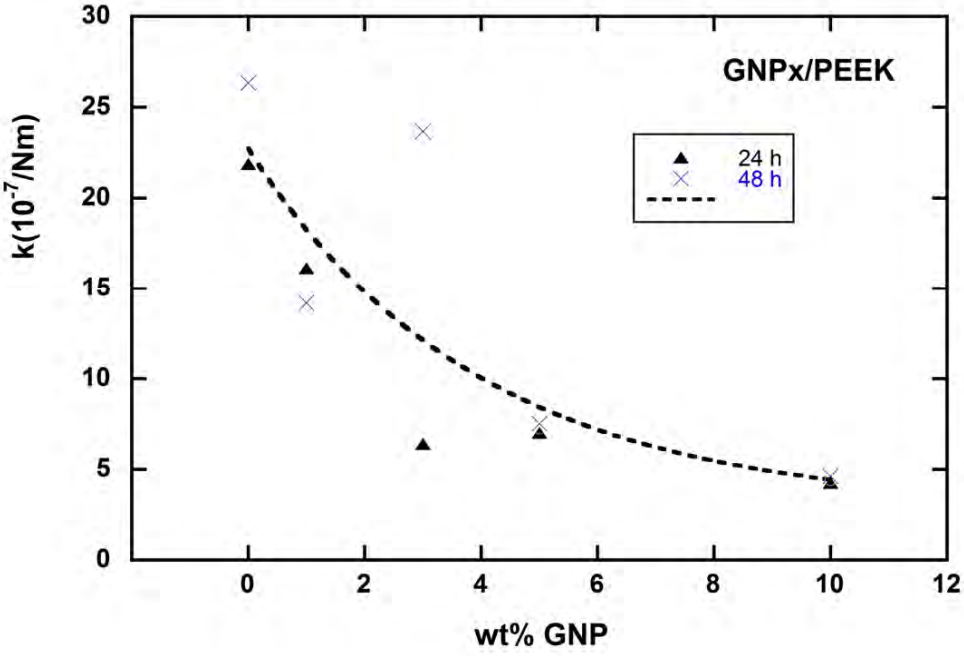

(c)

FIGURE 10. SEM images of the neat PEEK specimen: a) worn surfaces into the wear track after 48 h of wear process; b) a worn surface into the wear track after 48 h of wear process; and c) a zone far from the bearing contact.

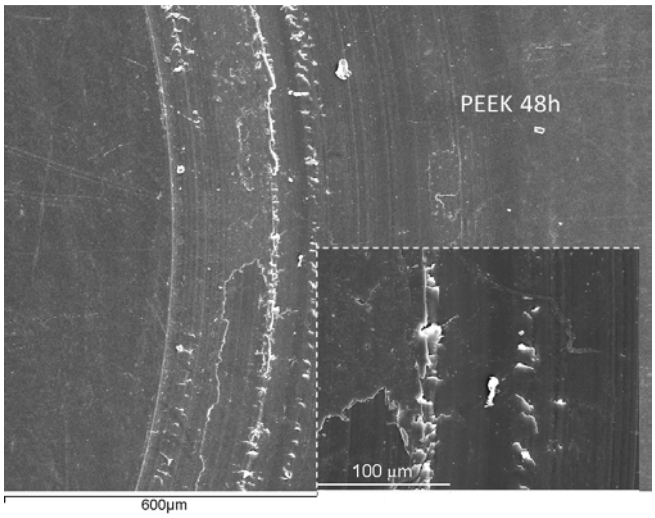

(a)

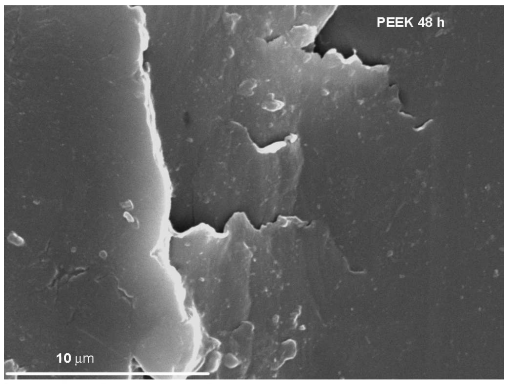

(b)

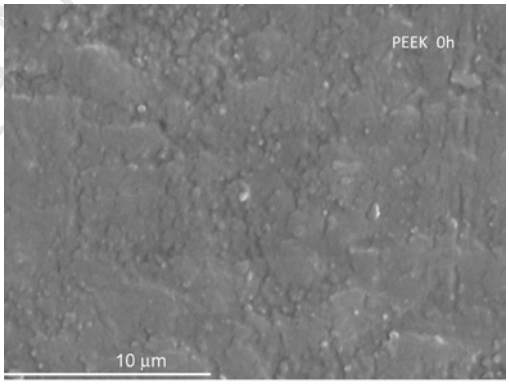

(c)

FIGURE 11. SEM images of the surface of the tribometer Al_2O_3 ball counterpart: a) before any wear process, b) after the wear process on neat PEEK, and c) after the wear process on GNP10/PEEK.

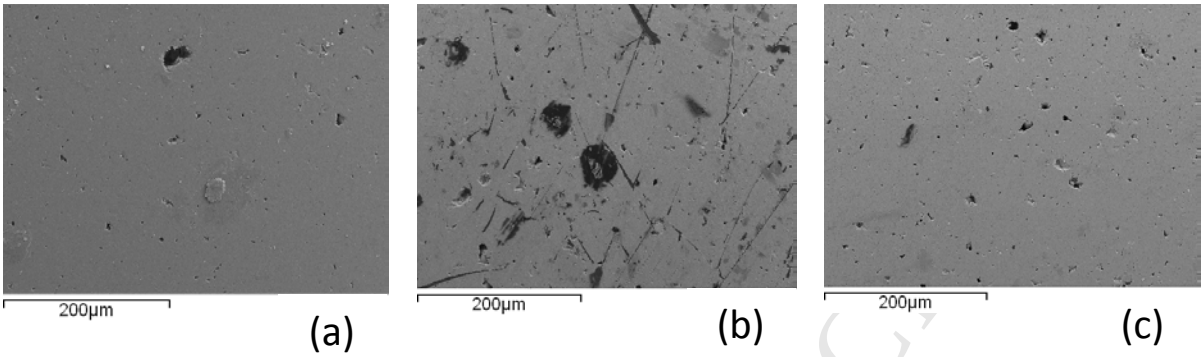

FIGURE 12. SEM images of worn surfaces on GNPx/PEEK composites after 24 h (a-d) and 48 h (e-h) of sliding: a,e) GNP1/PEEK; b,f) GNP3/PEEK; c,g) GNP5/PEEK; and d,h) GNP10/PEEK.

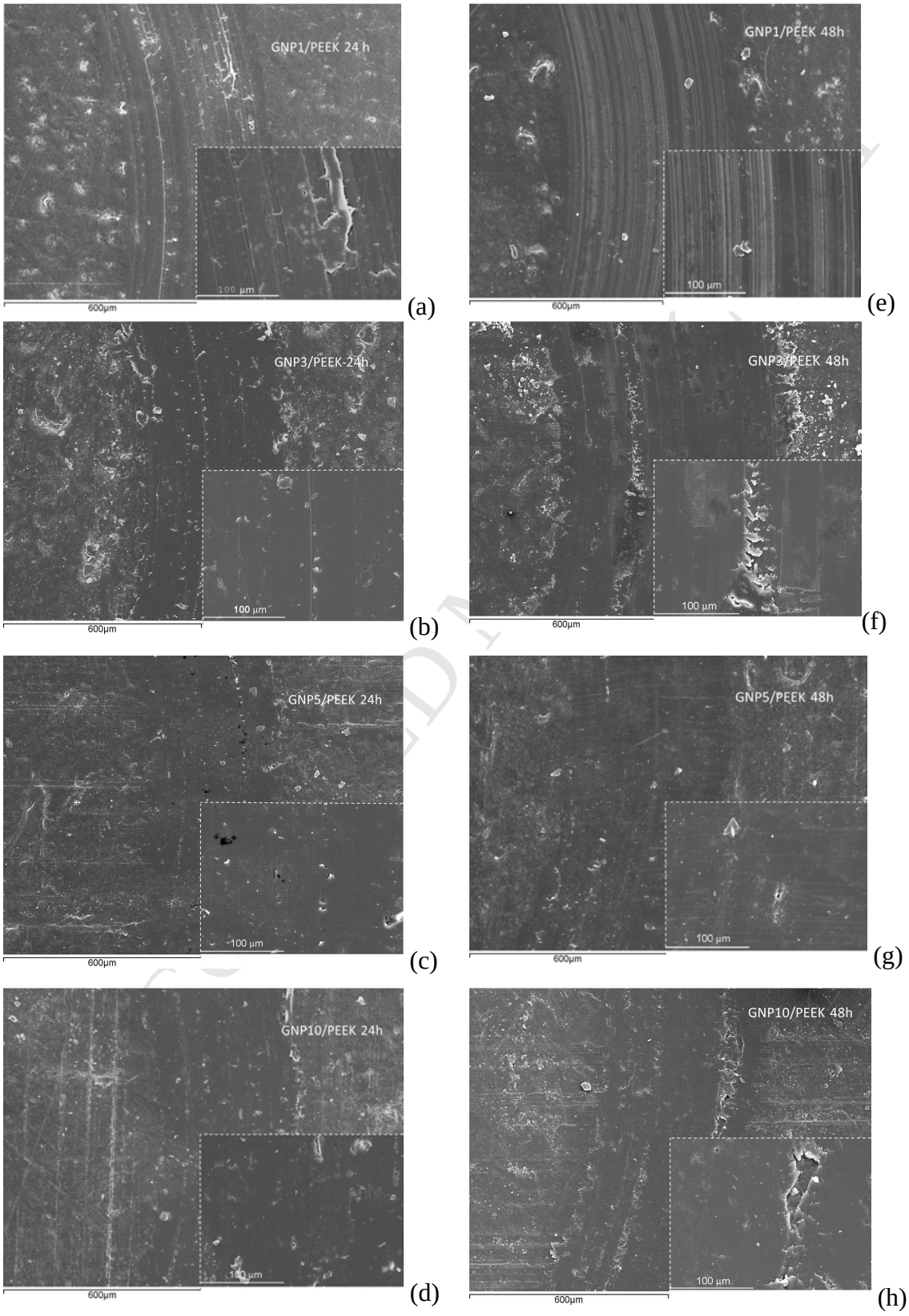

TABLE 1. DSC parameters for PEEK and GNPx/PEEK composites: ΔH_m = melting enthalpy; T_m = melting temperature; T_g = glass transition temperature; ΔH_c = crystallization enthalpy; and T_c = crystallization temperature.

wt%GNP	ΔH_m (J/g)[a]	T_m (K)	$T_{g,heat}$ (K)	ΔH_c (J/g)[a]	T_c (K)	$T_{g,cool}$ (K)
PEEK	51.4 ± 4	347.7 ± 1.0	—	54 ± 4.4	308.9 ± 0.1	146.1 ± 0.4
GNP1/PEEK	46.7 ± 1	347.7 ± 0.3	141 ± 2	52.3 ± 1.5	311.6 ± 0.3	143.9 ± 0.2
GNP3/PEEK	45.3 ± 1.1	348.0 ± 0.3	140.6 ± 1	53.3 ± 1.2	312.5 ± 0.5	142.9 ± 1.2
GNP5/PEEK	47.5 ± 3.9	347.6 ± 0.2	140 ± 1	54.9 ± 2.7	312.6 ± 0.3	143.3 ± 0.6
GNP10/PEEK	47.6 ± 3	348.0 ± 0.2	141.8 ± 1	56 ± 2.8	313.2 ± 0.3	142.4 ± 1

(a) The reported enthalpy contents are given per gram of PEEK

TABLE 2. Mechanical parameters obtained by uniaxial tensile stress: E = Young's modulus; σ_{TS} = ultimate tensile strength; ε^* = deformation of fracture; W = work of fracture (toughness).

Material	E (GPa)	σ_{TS} (MPa)	ε^* (%)	W (MJ/m^3)
PEEK	3.61 ± 0.08	105.6 ± 2.1	20.1 ± 1.5	18.1 ± 1.5
GNP1/PEEK	3.71 ± 0.29	98.6 ± 5.2	8.2 ± 0.5	7.0 ± 0.6
GNP3/PEEK	3.86 ± 0,44	96.5 ± 5.5	4.5 ± 0.4	4.2 ± 0.3
GNP5/PEEK	3.81 ± 0.50	95.4 ± 7.2	4.4 ± 0.3	4.0 ± 0.3
GNP10/PEEK	5.20 ± 0.51	88.5 ± 4.2	2.2 ± 0.3	1.6 ± 0.2

TABLE 3. Mechanical parameters obtained by 3-points bending test: E_b = flexural modulus; σ_b = flexural strength; ε^* = fracture strain; W_b = flexural work of fracture (toughness).

Material	E_b (GPa)	σ_b (MPa)	ε^*(%)	W_b (MJ/m^3)
PEEK	3.11 ± 0.19	-166.2 ± 2.4	-30.3 ± 0.2	40.0 ± 2.5
GNP1/PEEK	3.38 ± 0.08	-164.1 ± 1.6	-8.6 ± 0.2	9.4 ± 0.4
GNP3/PEEK	3.51 ± 0.10	-151.3 ± 4.3	-6.7 ± 0.3	6.3 ± 0.5
GNP5/PEEK	3.45 ± 0.11	-145.5 ± 3.1	-6.3 ± 0.3	5.6 ± 0.4
GNP10/PEEK	3.76 ± 0.22	-132.6 ± 3.4	-5.2 ± 0.2	4.1 ± 0.1

REFERENCES

[1] S.M. Kurtz, PEEK Biomaterials Handbook, Elsevier, Oxford, 2012, p. 298.
[2] A.S. Mohammed, M.I. Fareed, Improving the friction and wear of poly-ether-etherketone (PEEK) by using thin nano-composite coatings, Wear 364 (2016) 154-162.
[3] D.L. Burris, W.G. Sawyer, Tribological behavior of PEEK components with compositionally graded PEEK/PTFE surfaces, Wear 262(1-2) (2007) 220-224.
[4] E.Z. Li, W.L. Guo, H.D. Wang, B.S. Xu, X.T. Liu, Research on Tribological Behavior of PEEK and Glass Fiber Reinforced PEEK Composite, Physcs Proc 50 (2013) 453-460.
[5] W.R. Walsh, M.H. Pelletier, N. Bertollo, C. Christou, C. Tan, Does PEEK/HA Enhance Bone Formation Compared With PEEK in a Sheep Cervical Fusion Model?, Clin Orthop Relat R 474(11) (2016) 2364-2372.
[6] A. Wang, R. Lin, V.K. Polineni, A. Essner, C. Stark, J.H. Dumbleton, Carbon fiber reinforced polyether ether ketone composite as a bearing surface for total hip replacement, Tribology International 31(11) (1998) 661-667.
[7] W.Z. Nie, The effect of carbon nanotubes on the tribological behaviors of PEEK composites, Manufacturing Science and Technology, Pts 1-3 295-297 (2011) 140-143.
[8] A.M. Diez-Pascual, M. Naffakh, J.M. Gonzalez-Dominguez, A. Anson, Y. Martinez-Rubi, M.T. Martinez, B. Simard, M.A. Gomez, High performance PEEK/carbon nanotube composites compatibilized with polysulfones-I. Structure and thermal properties, Carbon 48(12) (2010) 3485-3499.
[9] A.M. Diez-Pascual, M. Naffakh, J.M. Gonzalez-Dominguez, A. Anson, Y. Martinez-Rubi, M.T. Martinez, B. Simard, M.A. Gomez, High performance PEEK/carbon nanotube composites compatibilized with polysulfones-II. Mechanical and electrical properties, Carbon 48(12) (2010) 3500-3511.
[10] C. Lee, X.D. Wei, J.W. Kysar, J. Hone, Measurement of the elastic properties and intrinsic strength of monolayer graphene, Science 321(5887) (2008) 385-388.
[11] I.W. Frank, D.M. Tanenbaum, A.M. Van der Zande, P.L. McEuen, Mechanical properties of suspended graphene sheets, J Vac Sci Technol B 25(6) (2007) 2558-2561.
[12] P.A. Denis, Density Functional Investigation of Thioepoxidated and Thiolated Graphene, Journal of Physical Chemistry C 113(14) (2009) 5612-5619.
[13] D. Berman, A. Erdemir, A.V. Sumant, Graphene: a new emerging lubricant, Mater Today 17(1) (2014) 31-42.
[14] B. Vasic, A. Matkovic, U. Ralevic, M. Belic, R. Gajic, Nanoscale wear of graphene and wear protection by graphene, Carbon 120 (2017) 137-144.
[15] Y.F. Mo, M.L. Yang, Z.X. Lu, F.C. Huang, Preparation and tribological performance of chemically-modified reduced graphene oxide/polyacrylonitrile composites, Compos Part a-Appl S 54 (2013) 153-158.
[16] H. Wang, G.Y. Xie, Z.G. Zhu, Z. Ying, Y. Zeng, Enhanced tribological performance of the multi-layer graphene filled poly(vinyl chloride) composites, Compos Part a-Appl S 67 (2014) 268-273.
[17] X.Y. Ye, X.H. Liu, Z.G. Yang, Z.F. Wang, H.G. Wang, J.Q. Wang, S.R. Yang, Tribological properties of fluorinated graphene reinforced polyimide composite coatings under different lubricated conditions, Compos Part a-Appl S 81 (2016) 282-288.
[18] S. Bhargava, N. Koratkar, T.A. Blanchet, Effect of Platelet Thickness on Wear of Graphene-Polytetrafluoroethylene (PTFE) Composites, Tribol Lett 59(1) (2015).
[19] J.A. Puertolas, S.M. Kurtz, Evaluation of carbon nanotubes and graphene as reinforcements for UHMWPE-based composites in arthroplastic applications: A review, Journal of the mechanical behavior of biomedical materials 39 (2014) 129-145.

[20] M. Kalin, M. Zalaznik, S. Novak, Wear and friction behaviour of poly-ether-ether-ketone (PEEK) filled with graphene, WS2 and CNT nanoparticles, Wear 332 (2015) 855-862.
[21] H.J. Song, N. Li, Y.J. Li, C.Y. Min, Z. Wang, Preparation and tribological properties of graphene/poly(ether ether ketone) nanocomposites, Journal of Materials Science 47(17) (2012) 6436-6443.
[22] L. Liu, F. Yan, F.Y. Gai, L.H. Xiao, L. Shang, M. Li, Y.H. Ao, Enhanced tribological performance of PEEK/SCF/PTFE hybrid composites by graphene, Rsc Adv 7(53) (2017) 33450-33458.
[23] A. Tewatia, J. Hendrix, Z.Z. Dong, M. Taghon, S. Tse, G. Chiu, W.E. Mayo, B. Kear, T. Nosker, J. Lynch, Characterization of melt-blended graphene - poly(ether ether ketone) nanocomposite, Mater Sci Eng B-Adv 216 (2017) 41-49.
[24] Proceeding of 3rd International PEEK Meeting, Washington, 2017.
[25] S.Z.D. Cheng, M.Y. Cao, B. Wunderlich, Glass-Transition and Melting Behavior of Poly(Oxy-1,4-Phenyleneoxy-1,4-Phenylenecarbonyl-1,4-Phenylene), Macromolecules 19(7) (1986) 1868-1876.
[26] A. Jonas, R. Legras, Relation between Peek Semicrystalline Morphology and Its Subglass Relaxations and Glass-Transition, Macromolecules 26(4) (1993) 813-824.
[27] H.S. Lee, W.N. Kim, Glass transition temperatures and rigid amorphous fraction of poly(ether ether ketone) and poly(ether imide) blends, Polymer 38(11) (1997) 2657-2663.
[28] B.S. Hsiao, B.B. Sauer, Glass-Transition, Crystallization, and Morphology Relationships in Miscible Poly(Aryl Ether Ketones) and Poly(Ether Imide) Blends, J Polym Sci Pol Phys 31(8) (1993) 901-915.
[29] Y.S. Chun, Y.S. Han, J.C. Hyun, W.N. Kim, Class transition temperatures and rigid amorphous fraction of poly(ether ether ketone) and polyarylate blends, Polymer 41(24) (2000) 8717-8720.
[30] G. Lewis, Contact stress at articular surfaces in total joint replacements. Part I: Experimental methods, Bio-Med Mater Eng 8(2) (1998) 91-110.
[31] G. Ellis, M. Naffakh, C. Marco, P.J. Hendra, Fourier transform Raman spectroscopy in the study of technological polymers Part 1: poly(aryl ether ketones), their composites and blends, Spectrochim Acta A 53(13) (1997) 2279-2294.
[32] B.J. Briscoe, B.H. Stuart, P.S. Thomas, D.R. Williams, A Comparison of Thermal-Induced and Solvent-Induced Relaxation of Poly(Ether Ether Ketone) Using Fourier-Transform Raman-Spectroscopy, Spectrochim Acta A 47(9-10) (1991) 1299-1303.
[33] N.J. Everall, J. Lumsdon, J.M. Chalmers, The Use of Polarized Fourier-Transform Raman-Spectroscopy in Morphological-Studies of Uniaxially Oriented Peek Fibers - Some Preliminary-Results, Spectrochim Acta A 47(9-10) (1991) 1305-1311.
[34] B.H. Stuart, A Fourier transform Raman spectroscopy study of the crystallisation behaviour of a poly-(ether ether ketone)/poly(ether sulphone) blend, Spectrochim Acta A 53(1) (1997) 107-110.
[35] T.Q. Li, M.Q. Zhang, L. Song, H.M. Zeng, Friction induced mechanochemical and mechanophysical changes in high performance semicrystalline polymer, Polymer 40(16) (1999) 4451-4458.
[36] M. Regis, A. Bellare, T. Pascolini, P. Bracco, Characterization of thermally annealed PEEK and CFR-PEEK composites: Structure-properties relationships, Polym Degrad Stabil 136 (2017) 121-130.
[37] D.R. Rueda, F. Ania, A. Richardson, I.M. Ward, F.J.B. Calleja, X-Ray-Diffraction Study of Die Drawn Poly(Aryletherketone) (Peek), Polym Commun 24(9) (1983) 258-260.
[38] B. Yazdani, Y.D. Xia, I. Ahmad, Y.Q. Zhu, Graphene and carbon nanotube (GNT)-reinforced alumina nanocomposites, J Eur Ceram Soc 35(1) (2015) 179-186.

[39] P. Cebe, S.Y. Chung, S.D. Hong, Effect of Thermal History on Mechanical-Properties of Polyetheretherketone Below the Glass-Transition Temperature, J Appl Polym Sci 33(2) (1987) 487-503.
[40] D.E. Spahr, J.M. Schultz, Determination of Matrix Crystallinity of Composites by X-Ray-Diffraction, Polym Composite 11(4) (1990) 201-210.
[41] Z.W. Wu, Y.B. Zheng, H.X. Yu, M. Seki, R. Yosomiya, Effect of Thermal History on Crystallization Behavior of Polyetheretherketone Studied by Differential Scanning Calorimetry, Angew Makromol Chem 164 (1988) 21-34.
[42] E.G. Lovering, Transcrystallinity and X-Ray Diffraction in Trans-1,4-Polyisoprene, J Polym Sci A2 8(10) (1970) 1697-&.
[43] B. Fragneaud, K. Masenelli-Varlot, A. Gonzalez-Montiel, M. Terrones, J.Y. Cavaille, Mechanical behavior of polystyrene grafted carbon nanotubes/polystyrene nanocomposites, Composites Science and Technology 68(15-16) (2008) 3265-3271.
[44] M. Wang, K.P. Pramoda, S.H. Goh, Enhancement of the mechanical properties of poly (styrene-co-acrylonitrile) with poly(methyl methacrylate)-grafted multiwalled carbon nanotubes, Polymer 46(25) (2005) 11510-11516.
[45] W.M. Prest, F.J. Roberts, Enthalpy Recovery in Pressure-Vitrified and Mechanically Stressed Polymeric Glasses, Ann Ny Acad Sci 371(Oct) (1981) 67-86.
[46] J.D. Menczel, M. Jaffe, How did we find the rigid amorphous phase?, J Therm Anal Calorim 89(2) (2007) 357-362.
[47] R. Rastogi, W.P. Vellinga, S. Rastogi, C. Schick, H.E.H. Meijer, The three-phase structure and mechanical properties of poly(ethylene terephthalate), J Polym Sci Pol Phys 42(11) (2004) 2092-2106.
[48] P.T. Huo, P. Cebe, Temperature-Dependent Relaxation of the Crystal Amorphous Interphase in Poly(Ether Ether Ketone), Macromolecules 25(2) (1992) 902-909.
[49] M. Naffakh, A.M. Diez-Pascual, Nanocomposite biomaterials based on poly(ether-ether-ketone) (PEEK) and WS2 inorganic nanotubes, J Mater Chem B 2(28) (2014) 4509-4520.
[50] S.R. Kim, D.H. Kim, D.J. Kim, M.H. Kim, J.M. Park, Study on thermal conductivity of polyetheretherketone/thermally conductive filler composites, Advances in Nanomaterials and Processing, Pts 1 and 2 124-126 (2007) 1079-+.
[51] C.L. Choy, K.W. Kwok, W.P. Leung, F.P. Lau, Thermal-Conductivity of Poly(Ether Ether Ketone) and Its Short-Fiber Composites, J Polym Sci Pol Phys 32(8) (1994) 1389-1397.
[52] A.A. Balandin, S. Ghosh, W.Z. Bao, I. Calizo, D. Teweldebrhan, F. Miao, C.N. Lau, Superior thermal conductivity of single-layer graphene, Nano Lett 8(3) (2008) 902-907.
[53] A. Li, C. Zhang, Y.F. Zhang, Thermal Conductivity of Graphene-Polymer Composites: Mechanisms, Properties, and Applications, Polymers-Basel 9(9) (2017).
[54] Y. Hwang, M. Kim, J. Kim, Improvement of the mechanical properties and thermal conductivity of poly(ether-ether-ketone) with the addition of graphene oxide-carbon nanotube hybrid fillers, Compos Part a-Appl S 55 (2013) 195-202.
[55] L. Liu, L.H. Xiao, X.P. Zhang, M. Li, Y.J. Chang, L. Shang, Y.H. Ao, Improvement of the thermal conductivity and friction performance of poly(ether ether ketone)/carbon fiber laminates by addition of graphene, Rsc Adv 5(71) (2015) 57853-57859.
[56] F.E. Alam, W. Dai, M.H. Yang, S.Y. Du, X.M. Li, J.H. Yu, N. Jiang, C.T. Lin, In situ formation of a cellular graphene framework in thermoplastic composites leading to superior thermal conductivity, J Mater Chem A 5(13) (2017) 6164-6169.
[57] K. Wu, C.X. Lei, R. Huang, W.X. Yang, S.G. Chai, C.Z. Geng, F. Chen, Q. Feng, Design and Preparation of a Unique Segregated Double Network with Excellent Thermal Conductive Property, Acs Applied Materials & Interfaces 9(8) (2017) 7637-7647.

[58] E. Pavlenko, F. Boyer, P. Puech, P. Olivier, A. Sapelkin, S. King, R. Heenan, F. Pons, B. Gauthier, P.H. Cadaux, W. Bacsa, Origin of mechanical modifications in poly (ether ether ketone)/carbon nanotube composite, J Appl Phys 115(23) (2014).
[59] L.L. Yang, S.L. Zhang, Z. Chen, Y.L. Guo, J.S. Luan, Z. Geng, G.B. Wang, Design and preparation of graphene/poly(ether ether ketone) composites with excellent electrical conductivity, Journal of Materials Science 49(5) (2014) 2372-2382.
[60] L.Y. Lin, H. Tlatlik, R. Gralla, M.A. Igartua, P. de Baets, A.K. Schlarb, Mechanical and thermal behaviours of polyetheretherketone-based multi-scale composites, J Compos Mater 47(17) (2013) 2087-2096.
[61] M.L. Di Lorenzo, M.C. Righetti, The three-phase structure of isotactic poly(1-butene), Polymer 49(5) (2008) 1323-1331.
[62] J.D. Badia, E. Stromberg, S. Karlsson, A. Ribes-Greus, The role of crystalline, mobile amorphous and rigid amorphous fractions in the performance of recycled poly (ethylene terephthalate) (PET), Polym Degrad Stabil 97(1) (2012) 98-107.
[63] A. Dahoun, M. Aboulfaraj, C. Gsell, A. Molinari, G.R. Canova, Plastic Behavior and Deformation Textures of Poly(Etherether Ketone) under Uniaxial Tension and Simple Shear, Polym Eng Sci 35(4) (1995) 317-330.
[64] V. Mittal, A.U. Chaudhry, Polymer - Graphene Nanocomposites: Effect of Polymer Matrix and Filler Amount on Properties, Macromol Mater Eng 300(5) (2015) 510-521.
[65] Q.L. Lin, L.J. Qu, Q.F. Lu, C.Q. Fang, Preparation and properties of graphene oxide nanosheets/cyanate ester resin composites, Polymer Testing 32(2) (2013) 330-337.
[66] Y.L. Li, S.J. Wang, Q. Wang, A molecular dynamics simulation study on enhancement of mechanical and tribological properties of polymer composites by introduction of graphene, Carbon 111 (2017) 538-545.
[67] H. Unal, A. Mimaroglu, Friction and wear characteristics of PEEK and its composite under water lubrication, J Reinf Plast Comp 25(16) (2006) 1659-1667.
[68] H.J. Kim, K.J. Seo, D.E. Kim, Investigation of Mechanical Behavior of Single- and Multi-Layer Graphene by using Molecular Dynamics Simulation, Int J Precis Eng Man 17(12) (2016) 1693-1701.
[69] S. Kawai, A. Benassi, E. Gnecco, H. Sode, R. Pawlak, X.L. Feng, K. Mullen, D. Passerone, C.A. Pignedoli, P. Ruffieux, R. Fasel, E. Meyer, Superlubricity of graphene nanoribbons on gold surfaces, Science 351(6276) (2016) 957-961.
[70] O. Jacobs, R. Jaskulka, C. Yan, W. Wu, On the effect of counterface material and aqueous environment on the sliding wear of carbon fibre reinforced polyetheretherketone (PEEK), Tribol Lett 19(4) (2005) 319-329.
[71] A. Chih, A. Anson-Casaos, J.A. Puertolas, Frictional and mechanical behaviour of graphene/UHMWPE composite coatings, Tribology International 116 (2017) 295-302.